WOOD RESEARCH doi.org/10.37763/wr.1336-4561/68.1.2843
ISSN 1336-4561 e-ISSN 2729-8906
68(1): 2023 28-43 pp.

MODELING THE EARLYWOOD AND LATEWOOD GROWTH RINGS OF NORWAY SPRUCE TIMBER BEAMS FOR FINITE ELEMENT CALCULATION

TAMÁS KIRÁLY, ZSOLT KARÁCSONYI, RUDOLF POLGÁR
UNIVERSITY OF SOPRON
HUNGARY

(RECEIVED SEPTEMBER 2022)

ABSTRACT

The purpose of this research is to determine the orthotropic material properties of the Norway spruce (*Picea abies*) and to develop a finite element modeling technique that, when applied to an individual specimen, can properly predict the outcome of the measurement results (i.e., deflection by a predefined loading) by simulation only. For the development of the finite element model of timber beams, their unique annual ring pattern is considered. The HSV color spectrum of picture of the end grain pattern is analyzed with a photo analytical algorithm in order to separate the phases, earlywood and latewood. The determined surface ratio of the phases is used to hypothesize that the volume and surface ratios are equal. For the description of wood as a material the rule of mixtures is used. The results of the compared measurements and FE models based on the introduced hypotheses show good agreement within the linear elastic limit.

KEYWORDS: Finite element method (FEM), 4-point bending test, earlywood and latewood, orthotropic material, rule of mixtures (ROM).

INTRODUCTION

Many researchers took a two-phased wood model into account by investigating the annual rings, the earlywood and latewood. Depending on the purpose, researchers carried out studies at the micro scale, the cells and its structure (Modén and Berglund 2008, Salmén and Megistris 2008, Qing and Mishnaevsky 2010) and at meso or macro scale, so they consider the bulk itself with or without annual rings (Fleischmann 2005, Qing and Mishnaevsky 2010, Sandhaas and van de Kuilen 2013, Gereke et al. 2015, Shao et al. 2020, Moshtaghin et al. 2021). Some researchers have found it obsolete to take into account the annual rings of the wooden beams and claim to have obtained good results by considering other kind of abstractions (Zhu 2014, Gecys et al. 2015, Saad and Lengyel 2021). According to Qing and Mishnaevsky Jr. (2010), not taking into

account the structure of the softwood by distinguishing just low density (earlywood) and high density (latewood) regions, leads to an oversimplification.

In the past years many computational models of wood were developed (Modén and Berglund 2008, Ormarsson et al. 2008, Qing and Mishnaevsky 2010). The earlywood and latewood are treated as homogeneous, but the bulk is considered as a composite material, thus heterogeneous. The challenge is to distinguish regions governed by having earlywood and latewood in the bulk in focus, and nevertheless to determine the material properties of earlywood and latewood.

The macroscopic properties of wood, such as density, hardness and other properties, are derived from the cells that make up the wood. There is a strong relationship between density and strength of the wood (Ross 2010). The earlywood is the portion of the growth ring that is formed during the early part of the growing season. It is usually less dense and weaker mechanically than latewood. The latewood is the portion of the growth ring that is formed after the earlywood formation has ceased. It is usually denser and stronger mechanically than earlywood. The wood as a material has a cylindrical symmetry (Szalai 1994). Its longitudinal direction is along the axis, while radial and tangential directions are in the transverse plane. The longitudinal modulus E_L of wood is over 10 times larger than the radial modulus E_R or tangential modulus E_T, whereas the radial and tangential modulus is considered similar but the difference should not be ignored. Therefore, wood may be described as an orthotropic material and its three mutually perpendicular axes are (Ross 2010). The longitudinal direction (axis "L") is parallel to the fiber (grain), the radial direction (axis "R") is normal to the growth rings (perpendicular to the grain in the radial direction) and the tangential direction (axis "T") is perpendicular to the grain but tangent to the growth rings.

Material model

The purpose of this paper is to explicitly model earlywood and latewood in a meso scale, which means modelling timber beams with individual annual rings. Models of softwoods, that take into account more relevant levels of wood structure, offer a better understanding of the mechanical properties and strength of wood. Some kind of abstraction is needed to create a material model that describes wood as a complex material. The two main abstractions introduced in this paper are treated as hypotheses. To examine their reality base, measurement results were compared with the results of finite element models based on the hypotheses.

First hypothesis: surface ratio equals volume ratio

For predicting the mechanical properties of fiber reinforced materials the rule of mixtures (ROM) is used, as a weighted mean. In broadest definition a composite is a combination of at least two constituents (Isaac and Ori 2006). Considering wood as a composite material because of the annual rings, the formulas of the fiber reinforced materials can be reinterpreted to the earlywood and latewood. Some also considered the micromechanical properties on different scale levels from microfibrils to annual rings (Qing and Mishnaevsky 2010). In the further investigation we should restrict ourselves to determine the characteristics of the earlywood and latewood in a semi-empirical way.

The following general formula defines the composition of a mixture with a dimensionless quantity (Warnet and Akkerman 2008, Eq. 2.1-3):

$$\sum_{i=1}^{n} v_i = 1 \quad \text{with} \quad v_i = \frac{V_i}{V_c} \tag{1}$$

where: v_i is the volume fraction of the i-th constituent, V_i is the volume of the i-th constituent, V_c is the total volume of the composite. The similar rule for mass content by substituting the product of density and volume leads to (Warnet and Akkerman 2008, Eq. 2.1-4):

$$\rho_c = \sum_{i=1}^{n} \rho_i \, v_i \tag{2}$$

Now rewriting the formula of the relative content of the earlywood and latewood:

$$v_{EW} + v_{LW} = 1 \tag{3}$$

$$\overline{\rho} = \rho_{EW} \cdot v_{EW} + \rho_{LW} \cdot v_{LW} \tag{4}$$

where: $\overline{\rho}$ is the average density of analyzed wooden structure (this value can be easily measured), v_{EW}, ρ_{EW} is the relative volume and density of the earlywood respectively and v_{LW}, ρ_{LW} is the relative volume and density of the latewood respectively.

Hypothesis 1: For class A (highest quality class) or class B wood we assume, that proportion of earlywood and latewood in the end cross-section of the analyzed beam nearly equals in all cross-sections along its longitudinal axis. This assumption leads to:

$$V = L \cdot (A_{EW} + A_{LW}) = L \cdot \left(\sum_{i=1}^{n} \alpha_i^{EW} \cdot r_i^{EW} \cdot t_i^{EW} + \sum_{i=1}^{m} \alpha_i^{LW} \cdot r_i^{LW} \cdot t_i^{LW} \right) \quad \text{with } n, m \gg 1 \tag{5}$$

where: n and m is the number of earlywood and latewood rings, r_i is the radius of the i-$_{th}$ ring, t_i is the thickness of the i-th ring and α refers to the angle of the arc length corresponding to the i-th ring. If n and m is high enough, it can be assumed the amount of earlywood and latewood rings is equal and the Eq. 5 can be further simplified.

The density of the earlywood and latewood rings can be determined by measuring finite small specimens or one can accept the experimental values of other experiments. If the assumptions are good enough, the given formula should lead to the measured weight of the beam.

Second hypothesis: ROM combined with the correlation between the orthotropic material properties and density of earlywood and latewood

The ROM is used for establishing a connection between the composite bulk and its two phases, the earlywood and latewood. The two basic models used for linear elastic materials are the Voigt's and Reuss models. The Fig. 1 is valid for the two-phase composite materials.

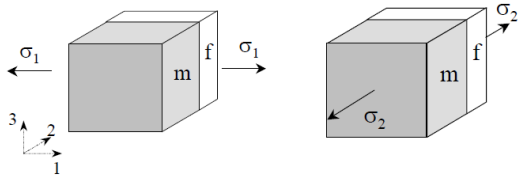

Fig. 1: Voigt's (left) and Reuss-model (right) (Warnet and Akkerman 2008).

The longitudinal modulus E_L and tangential modulus E_T are obtained by considering that earlywood and latewood rings are in parallel. The average stress $\sigma_{L/T}$ in the cross-section is:

$$\sigma_{L/T} = \sigma_{EW,L/T} \cdot v_{EW} + \sigma_{LW,L/T} \cdot v_{LW} \quad (6)$$

According to the strain energy approach and by acknowledging the orthotropic character of the earlywood and latewood, the strains induced in both are equal:

$$E_{L/T} \cdot \epsilon_{L/T} = E_{EW,LT} \cdot \epsilon_{EW,L/T} \cdot v_{EW} + E_{LW,L/T} \cdot \epsilon_{LW,L/T} \cdot v_{LW} \quad (7)$$

The radial modulus E_R is obtained by considering that earlywood and latewood rings are in series. The deformation ϵ_R is the sum of the deformation of the earlywood and latewood rings:

$$\epsilon_R = \epsilon_{EW,R} \cdot v_{EW} + \epsilon_{LW,R} \cdot v_{LW} \quad (8)$$

For linear-elastic material using the Hooke's law, it can be written as:

$$\frac{\sigma_R}{E_R} = \frac{\sigma_{EW,R} \cdot v_{EW}}{E_{EW,R}} + \frac{\sigma_{LW,R} \cdot v_{LW}}{E_{LW,R}} \quad (9)$$

In case of the Reuss-model the stresses σ_R, $\sigma_{EW,R}$ and $\sigma_{LW,R}$ are equal.

$$\frac{1}{E_R} = \frac{v_{EW}}{E_{EW,R}} + \frac{v_{LW}}{E_{LW,R}} \quad (10)$$

For the shear moduli, the approach of the radial modulus is used:

$$\frac{1}{G} = \frac{v_{EW}}{G_{EW}} + \frac{v_{LW}}{G_{LW}} \quad (11)$$

$$G = \frac{G_{EW} \cdot G_{LW}}{v_{LW} \cdot G_{EW} + v_{EW} \cdot G_{LW}} \quad (12)$$

Qing and Mishnaevsky Jr. (2010) doesn't mention any approach how to determine the ROM of shear moduli. According to some research results (Gereke et al. 2015), there is no need for the ROM to be used to determine the Poisson's ratios. The same Poisson's ratios can be applied to earlywood and latewood as well. The formulas proposed so far allow determination of material properties of the analyzed wooden beams if the properties of the two phases, earlywood and latewood, are known. These equations give the ROM-relation for the orthotropic material parameters.

If the material properties of wood as a composite of earlywood and latewood are unknown, the proposed way of solution has to be inverted to calculate the unknown values. Yet there is a need to obtain more equations to describe the relationship between earlywood and latewood.

Jernkvist and Thuvander (2001) used an optical method, called digital speckle photography (DSP), to measure the radial dependence of material properties of Norway spruce. The DSP is well suited for measurements on objects with small details, since the method can be combined with microscopy.

Hypothesis 2: rules of mixtures combined (Eqs. 13-15) with the correlation between the orthotropic material properties and density of earlywood and latewood lead to Eqs. 16-22. The following considerations of obtaining stiffness relations for the Norway spruce are taking into account the difference between the cells of earlywood and latewood (as a macroscopic model) while referencing on other publications with experimental values. The ROM-relation of the longitudinal and tangential modulus:

$$E_{L/T} = E_{EW,L/T} \cdot v_{EW} + E_{LW,\frac{L}{T}} \cdot v_{LW} \tag{13}$$

After the rearrangement of the Eq. 10, the following equation gives the ROM-relation of the radial modulus:

$$E_R = \frac{E_{EW,R} \cdot E_{LW,R}}{v_{LW} \cdot E_{EW,R} + v_{EW} \cdot E_{LW,R}} \tag{14}$$

The ROM-relation of the shear moduli:

$$G = \frac{G_{EW} \cdot G_{LW}}{v_{LW} \cdot G_{EW} + v_{EW} \cdot G_{LW}} \tag{15}$$

The Poisson's ratios of the earlywood and latewood are considered equal.

The Eqs. 16-22 define the stiffness relations for the Norway spruce between earlywood and latewood. Gibson and Ashby (1997) observed a linear relation between density and longitudinal modulus $\mathbf{E_L}$ (Eq. 16). Gibson and Ashby (1997) and Nairn (2006) predicted that tangential modulus scales with the cube of density (Eq. 17). Recent publication from Modén and Berglund (2008) propose a scaling of the radial modulus less than cubic, also like in Nairn (2006) (Eq. 18). Measuring the shear moduli by generating pure shear deformation state, comes with great difficulty. Gibson and Ashby (1997) observed a cubic relation between density, $\mathbf{G_{RT}}$ and $\mathbf{E_L}$, a linear relation between density, $\mathbf{G_{TL/RL}}$ and $\mathbf{E_L}$, (Eqs. 19, 20). Other publications, e.g. (Qing and Mishnaevsky 2010), suggest to select a reasonable value like the one of the bulk or empirical values obtained through parameter studies of earlywood and latewood.

The Poisson's ratios $\mathbf{\nu_{EW/LW,TL}}$ and $\mathbf{\nu_{EW/LW,RL}}$ have very small values and their determination (Eq. 21) is less precise than for $\mathbf{\nu_{TR}}$ (Ross 2010). The DSP measurements of Jernkvist and Thuvander (2001) showed the inequality of $\mathbf{\nu_{EW,RT}}$ and $\mathbf{\nu_{LW,RT}}$. Due the lack of a more precise determination these values, in this paper the Poisson's ratios in Eq. 22 are considered as equal.

$$E_{LW,L} = E_{EW,L} \cdot \left(\frac{\rho_{LW}}{\rho_{EW}}\right) \quad (16)$$

$$E_{LW,T} = E_{EW,T} \cdot \left(\frac{\rho_{LW}}{\rho_{EW}}\right)^3 \quad (17)$$

$$E_{EW,R} = E_{LW,R} \cdot \left(\frac{\rho_{LW}}{\rho_{EW}}\right)^{1.63} \quad (18)$$

$$G_{LW,RT} = G_{EW,RT} \cdot \left(\frac{\rho_{LW}}{\rho_{EW}}\right)^3 \quad (19)$$

$$G_{LW,TL/RL} = G_{EW,TL/RL} \cdot \left(\frac{\rho_{LW}}{\rho_{EW}}\right) \quad (20)$$

$$\nu_{EW,\mathrm{TL/RL}} = \nu_{LW,\mathrm{TL/RL}} = \nu_{\mathrm{TL/RL}} \quad (21)$$

$$\nu_{LW,RT} \sim \nu_{EW,RT} \qquad \text{(but in the reality } \nu_{LW,RT} > \nu_{EW,RT}\text{)} \quad (22)$$

In the following only linear material behavior of wood is considered. This means nonlinearities in material properties, such as different stiffness values in tension and compression parallel to grain are not taken into account. However, this restriction is not necessary because of the material model presented. To guarantee the positive-definiteness of the elasticity tensor, the following conditions have to be fulfilled:

$$\nu_{LR}^2 < \frac{E_L}{E_R}, \qquad \nu_{LT}^2 < \frac{E_T}{E_L}, \qquad \nu_{RT}^2 < \frac{E_R}{E_T} \quad (23)$$

$$1 - \nu_{LR}^2 - \nu_{LT}^2 - \nu_{RT}^2 - 2 \cdot \nu_{LR} \cdot \nu_{LT} \cdot \nu_{RT} > 0 \quad (24)$$

MATERIAL AND METHODS

Measurement set-up

The experiments of 4-point bending test with timber beams were conducted in a laboratory accredited for timber structural testing (Andor et al. 2015). These destructive tests have been performed according to DIN EN 408-2012-10 (2012) using the material testing device FPZ-100 and a standard MTS testing device. The MTS testing device has a load capacity of 250 kN, which is about 50 times more than the ultimate load of the strongest specimens. The load was applied by a single actuator and transmitted to the centrally aligned specimen with a rate of 5 mm·min^{-1}. The measurement of the deflection at the middle of the timber beam has been performed with a videoextensometer, which was connected to a computer storing all the recorded data, like depicted on Fig. 2. Tab. 1 shows the measurement set-up of the specimens.

Tab. 1: Measurement set-up.

Specimens (mm)	**Span of pressure stamps**		**Radius of stamps** (mm)
	L_A (mm)	L_B (mm)	
20 x 20 x 400	120	360	15
40 x 40 x 800	230	650	15

All of the specimens were sawn of Norway spruce (*Picea abies*) in rectangular solid cross-sections and dried to a moisture content of 12%. The experiments were carried out at

a room temperature of 20°C. The orientation with respect to growth-rings were aligned to the contour in an angle about 20 to 60 deg. This was necessary in order to trigger a biaxial bending of the specimens, which effect could be analyzed with FE-models combined with a parameter analysis, helping to determine the orthotropic material properties of the timber.

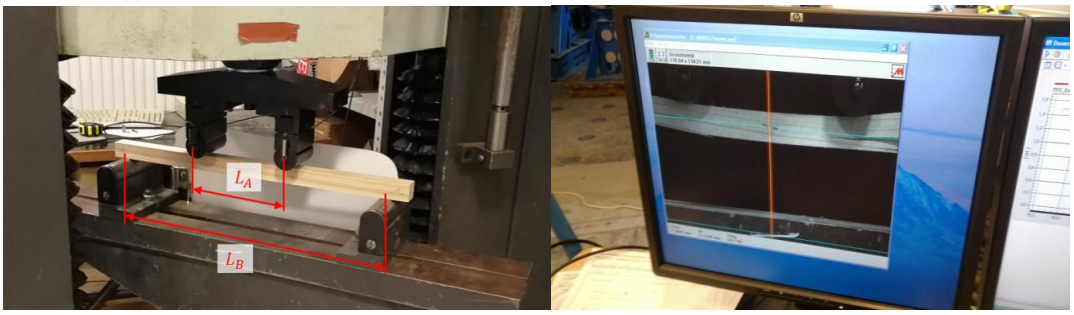

Fig. 2: a) 4-point bending test measurement set-up of the specimens, b) videoextensometer for non-contact measurement of strain and material parameters.

The idea of using 20 x 20 mm cross-sectioned beams (Fig. 3a) was based on ensuring with visual inspection (followed by a destructive test), that none of the specimens has a major visible defect, drying splits or even knots, which is a natural feature of the species. So, it can be stated, that the carefully selected specimens did not contain any major failures, which could have had an effect on the mechanical properties.

For the 40 x 40 mm specimens (Fig. 3b) the orientation of the growth-ring in the cross-sections weren't aligned as at the smaller specimens. Via visual inspection and non-destructive tests, it was ensured that none of the specimens used for the experiments had major defects, yet the presence of small knots was allowed. Slightly damaged end-cross-sections (like specimen 10, damaged on both sides) require to extrapolate beyond the range of acquirable information.

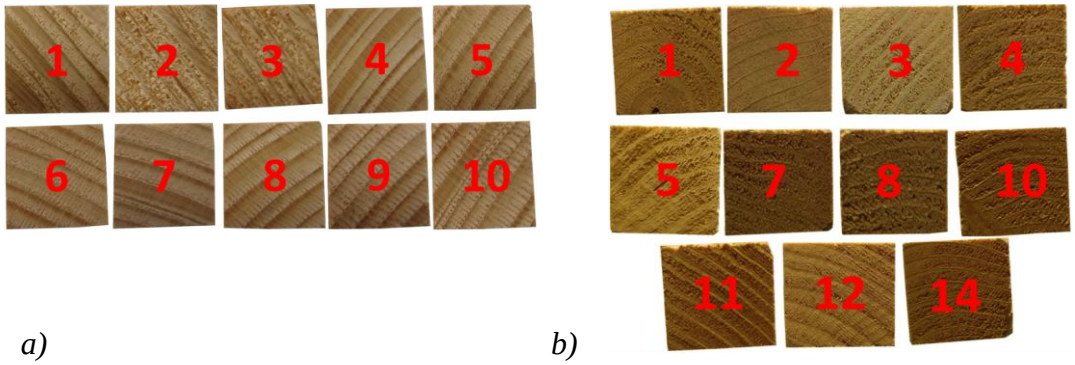

a) *b)*

Fig. 3: a) End grains of the 20 x 20 specimens, b) end grains of the 40 x 40 specimens.

Finite element model of timber beams

Linear elastic orthotropic material properties of earlywood and latewood

For the analyzes the values in (Tab. 2) were used, which are based on the studies of (Qing and Mishnaevsky 2010, Fleischmann 2005, Nilsen 2015, Khokhar et al. 2010) and the experiments carried out for this paper. In Tab. 2 not all of the values of earlywood and

latewood are experimental results (like the Poisson's ratios), they are however reasonable values, which are consistent with the bulk properties. The values of Tab. 2 are considered for 45% volume ratio of latewood in the bulk.

Tab. 2: Material properties of earlywood and latewood used for the analyzes.

Material constants	Symbol	Unit	Bulk	Earlywood (EW)	Latewood (LW)	Exponent
Density	$\rho_{EW/LW}$	kg·m^{-3}	-	215	820	-
Long. modulus	$E_{EW/LW,L}$	MPa	11286	4979.969	18993.371	1
Rad. modulus	$E_{EW/LW,R}$	MPa	960	576.735	5112.323	1.63
Tang. modulus	$E_{EW/LW,T}$	MPa	620	24.299	1348.079	3
Poisson's ratio LR	$\nu_{EW/LW,LR}$	-	0.041	0.041	0.041	-
Poisson's ratio LT	$\nu_{EW/LW,LT}$	-	0.033	0.033	0.033	-
Poisson's ratio RT	$\nu_{EW/LW,RT}$	-	0.35	0.35	0.35	-
Shear modulus LR	$G_{EW/LW,LR}$	MPa	580	387.433	1477.651	1
Shear modulus LT	$G_{EW/LW,LT}$	MPa	590	394.113	1503.128	1
Shear modulus RT	$G_{EW/LW,RT}$	MPa	80	44.649	2477.062	3

Modeling the cross-section

The analyses were done by creating a mesh of the shape of the timber beam that contains information about the material. The FE models were created based on photos of the end grains of the specimens. There are three main steps in order to obtain a meshed model for the FE analysis (Fig. 4): *(1)* Shooting a macro photo, so that all the details and pattern of the annual rings are well recognizable. After the photo was taken, a photo analytic processing tool of (Polgár 2017) was used for analyzing the color spectrum (HSV color model) and for detecting the end grain on the picture. A modified version of the same tool was used to separate earlywood and latewood. *(2)* Using the bi-colored pictures 2-D surfaces are generated for each earlywood and latewood growth ring as shown in Fig. 4. The skewed surfaces can be stretched to achieve a the real (maybe a bit imperfect) rectangular shape used for the FE calculations. *(3)* The obtained surfaces are meshed with a 2-D mesh which are extruded to achieve the final 3-D mesh of the beam. Next the material properties are defined and the measurement set-up (**Error! Reference source not found.**a) is realized in the FE-model in terms of boundary conditions and acting loads.

The modifications of the tool of (Polgár 2017) were the following: editable bandwidth of the color spectra, created splines can have an arbitrary form and not necessarily a circle shaped one, like written for its original purpose of detecting end grain area of the felled trees.

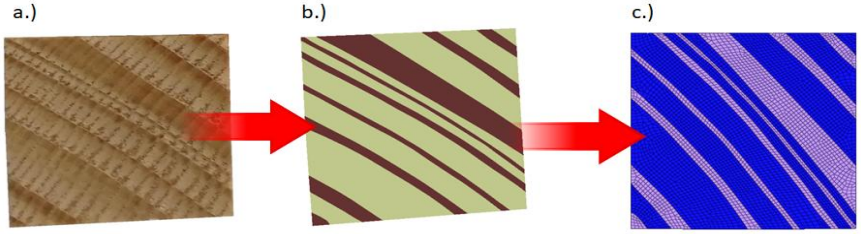

Fig. 4: Obtaining a FE-mesh from a picture of the end grain: a) photo of the end grain of the specimen, b) generated surfaces of earlywood and latewood, c) meshed surfaces of earlywood and latewood.

For the definition of orthotropic material properties, a local coordinate system is used with respect to the alignment of growth rings in the cross-section of each specimen. Wood properties are usually defined in a cylindrical (or polar) material coordinate system with the origin in the pith. In case the growth rings lie on a large radius, hence their alignment is approximately parallel to each other, a rectangular coordinate can be used (Fig. 5).

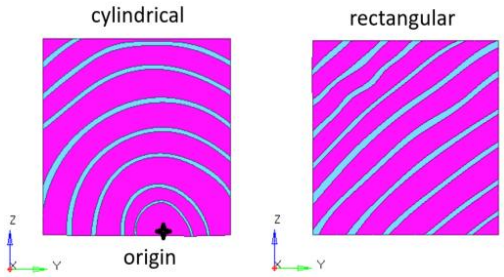

Fig. 5: Choice of local coordinate system depending on the alignment and size of the growth rings.

Elements, boundary conditions and loads

For this paper the FE models were only used to calculate structural deformation and stresses. Like mentioned before, the specimens are modeled with straight grain without any knots, holes or cracks. The created geometry is meshed with first order continuum elements C3D8I (8-node brick, hexahedral) (Abaqus 2014) as depicted in Fig. 6. The models satisfy the disciplines of linear elastic solver for quasistatic analysis, in respect to proper mesh quality, non-follower loading, small displacements and linear elastic material properties. For the analysis only "half"-models are used to decrease computing time and because the conditions of symmetry are fulfilled (Fig. 6).

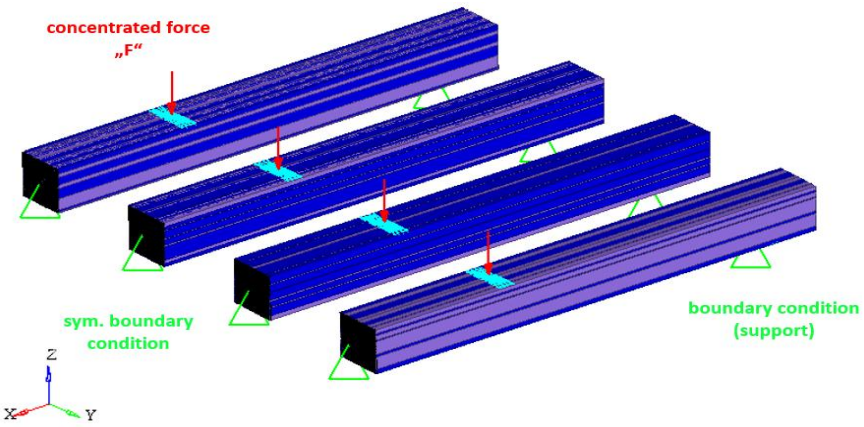

Fig. 6: Some of the FE models of the timber beams as example.

RESULTS AND DISCUSSION

Experiment results

For the experiment 20 x 20 beams shown in Tab. 3 a total of 10 specimens were prepared. The measured density of the given specimens gave an average 551.37 kg·m^{-3} with a relative

standard deviation of 50.19. The average ratio of the latewood proportion is 38.45% with a relative standard deviation of 6.70%.

For the 40 x 40 specimens, 14 pieces were prepared for measurements, see Tab. 4. Due to errors during the measurement of the specimen 6, 9 and 13 have no results available. The measured density of the given specimens gave an average 327.187 $kg \cdot m^{-3}$ with a relative standard deviation of 15.801. The average ratio of the latewood proportion is 19.00% with a relative standard deviation of 2.23%.

Tab. 3: Experiment results of the 20 x 20 specimens.

Nº	**Cross-section** (mm)	**Ratio of latewood**[1] (%)	**Weight** (g)	**Density** ($kg \cdot m^{-3}$)	**Max deflection** (mm)	**Ultimate load** (kN)	**Deflection by 0.5 kN** (mm)
1	19.54 x 20.18	43.68	98	621.33	11.642	1.585	2.889
2	19.52 x 19.93	36.51	79	507.67	9.744	1.523	2.377
3	19.61 x 20.15	28.46	74	468.19	12.280	1.529	2.751
4	19.67 x 19.85	48.63	97	621.08	12.876	1.619	3.224
5	19.69 x 20.23	32.68	81	508.37	14.578	1.644	3.047
6	19.73 x 20.33	29.61	84	523.55	17.423	1.727	2.839
7	20.12 x 19.81	42.65	93	583.32	16.957	1.763	2.927
8	19.74 x 20.13	44.69	89	559.94	12.616	1.543	2.994
9	19.79 x 20.22	37.86	88	549.79	18.064	1.761	3.312
10	19.78 x 20.16	39.74	91	570.51	12.804	1.625	3.139
***Ave**	19.72 x 20.10	38.45	87.40	551.37	13.901	1.632	2.951
****Std**	0.17 x 0.17	6.70	7.80	50.19	1.630	0.092	0.266

[1]The area of the late- and earlywood is calculated by the average areas at both ends of the timber beam specimen. *Ave- average, **Std- standard deviation.

Tab. 4: Experiment results of the 40 x 40 specimens.

Nº	**Cross-section** (mm)	**Ratio of latewood**[1] (%)	**Weight** (g)	**Density** ($kg \cdot m^{-3}$)	**Max deflection** (mm)	**Ultimate load** (kN)	**Deflection by 0.5 kN** (mm)
1	40.58 x 41.49	16.27	460	341.510	11.560	3.167	8.679
2	41.35 x 40.05	21.21	417	314.776	12.064	3.733	7.563
3	39.43 x 41.11	19.35	409	315.449	16.138	4.267	7.738
4	40.73 x 41.20	21.52	418	311.372	10.605	3.250	7.985
5	41.36 x 39.56	18.33	407	310.926	15.936	4.517	7.597
7	40.26 x 38.97	17.93	447	356.170	15.125	4.767	6.639
8	40.27 x 39.65	16.07	402	314.699	10.431	2.933	8.337
10	41.46 x 40.06	17.64	437	328.921	12.207	3.733	7.702
11	39.95 x 39.33	22.37	414	329.317	13.025	3.900	7.855
12	39.55 x 41.64	18.03	445	337.808	11.433	3.383	7.883
14	39.17 x 40.21	20.33	426	338.110	13.739	3.950	8.351
***Ave**	40.37 x 40.30	19.00	425.6	327.187	12.933	3.782	7.848
****Std**	0.85 x 0.97	2.23	20.0	15.801	2.156	0.608	0.562

[1]The area of the late- and earlywood is calculated by the average areas at both ends of the timber beam specimen. *Ave- average, **Std- standard deviation.

For the FE calculations, the densities of spruce timber had to be determined statistically. The earlywood has a density (ρ_{EW}) of 215 kg·m^{-3} and the latewood has a density (ρ_{LW}) of 820 kg·m^{-3}.

Comparison between FE and experimental results

For the measurements, quite a few parameters must be documented in addition to the force-deflection data. For example, the weight of the timber beam respective the photo of the end grain cross-section. Based on these, parameters can be calculated to measure the validity of simplification assumptions and modeling.

According to the Hypothesis 1 from the measured weight of the specimens, their average density can be obtained. These density values can be compared to the average density, which is calculated by using the assumptions and the annual ring ratio determined from the photos. According to the Hypothesis 2 the ROM combined with the correlation among the orthotropic material properties and density of earlywood and latewood, the material properties of the Norway spruce can be obtained (Tab. 2). The measured deflections at a given load can be compared with the deflections calculated with the finite element models.

A qualitative comparison between experimental data and FE results demonstrates good agreement. An overview of all results is shown in Tab. 5 and Tab. 6 respectively. Modeling results were satisfying in terms of stiffness, deflection and as well in control parameters like; measured and calculated mass of the specimens. Clearly the greatest deflection for 4-point bending test for symmetrical models is measured in the middle of the beams. Depending on the cross-sections a torsional twist can occur, in that case the average deflection in the middle cross-section is calculated.

For the 20 x 20 specimens the density errors range between -15% and -33%. The deviation of the calculated density values is due to the inaccurate detection of the earlywood and latewood ratio in the end grain. It seems that the ratio of latewood is generally underestimated by the photo analytic processing tool. In case of bending, the percentage errors range between 3% and 37%.

Tab. 5: Comparison of experiment and FE calculation results of the 20 x 20 x 400 specimens.

Nº	Max		Weight (g)	LW ratio (%)	Average density		Error (%)	Deflection by 0.5 kN		Error (%)
	Deflection (mm)	Force (N)			Measured (kg·m^{-3})	Calculated (kg·m^{-3})		Measured (mm)	Calculated (mm)	
1	11.642	1.585	43.68	43.68	621.327	479.264	-29.64	2.89	3.75	22.96
2	9.766	1.523	36.51	36.51	507.668	435.886	-16.47	2.38	2.77	14.19
3	12.280	1.529	28.46	28.46	468.187	387.183	-20.92	2.75	3.33	17.39
4	12.876	1.619	48.63	48.63	621.079	509.212	-21.97	3.22	3.31	2.72
5	14.578	1.644	32.68	32.68	508.374	412.714	-23.18	3.05	3.75	18.75
6	17.423	1.727	29.61	29.61	523.546	394.141	-32.83	2.84	4.49	36.74
7	16.957	1.763	42.65	42.65	583.325	473.033	-23.32	2.93	3.61	18.92
8	12.616	1.543	44.69	44.69	559.937	485.375	-15.36	2.99	3.45	13.22
9	18.064	1.761	37.86	37.86	549.789	444.053	-23.81	3.31	4.10	19.22
10	12.804	1.625	39.74	39.74	570.512	455.427	-25.27	3.14	3.41	7.92
***Ave**	13.901	1.632	38.45	38.45	551.374	441.585	-23.28	2.95	3.60	17.20
****Std**	2.754	0.092	6.70	6.70	50.187	34.403	5.30	0.27	0.47	9.10

For the 40 x 40 specimens the density errors are in the worst case between ± 10%. In case of bending, the percentage errors move on a slightly larger scale, in which case the values range between -9% and +16% percent. It can be stated that the 40 x 40 specimens generally lead to a better correlation of the measured and calculated values.

Stress distributions in the beam cross-sections are also of interest. Because of the absent of earlywood-latewood transitions, there are sharp changes in stresses between the layers. No transition zone between earlywood and latewood is considered.

Tab. 6: Comparison of experiment and FE-calculation results of the 40 x 40 x 800 specimens.

Nº	Max		Weight (g)	LW ratio (%)	Average density		Error (%)	Deflection by 0.5 kN		Error (%)
	Deflection (mm)	Force (N)			Measured ($kg \cdot m^{-3}$)	Calculated ($kg \cdot m^{-3}$)		Measured (mm)	Calculated (mm)	
1	11.560	3.167	460	16.27	341.510	313.417	-8.96	8.68	8.06	-7.69
2	12.064	3.733	417	21.21	314.776	343.330	8.32	7.56	7.54	-0.25
3	16.138	4.267	409	19.35	315.449	332.082	5.01	7.74	7.69	-0.63
4	10.605	3.250	418	21.52	311.372	345.186	9.80	7.99	7.63	-4.63
5	15.936	4.517	407	18.33	310.926	325.893	4.59	7.60	7.73	1.68
7	15.125	4.767	447	17.93	356.170	323.495	-10.10	6.64	7.88	15.74
8	10.431	2.933	402	16.07	314.699	312.216	-0.80	8.34	8.41	0.86
10	12.207	3.733	437	17.64	328.921	321.722	-2.24	7.70	8.10	4.89
11	13.025	3.900	414	22.37	329.317	350.338	6.00	7.86	7.25	-8.39
12	11.433	3.383	445	18.03	337.808	324.069	-4.24	7.88	7.87	-0.22
14	13.739	3.950	426	20.33	338.110	338.015	-0.03	8.35	7.65	-9.12
***Ave**	12.933	3.782	425.6	19.00	327.187	329.978	0.67	7.85	7.80	-0.71
****Std**	2.156	0.608	20.0	2.23	15.801	13.518	6.70	0.56	0.33	7.10

It is clear, that for 4-point bending tests the dominating stress is the longitudinal stress (Fig. 7a). The highest longitudinal stress magnitudes are present in the latewood layers and they are about 4 times higher than the ones in the earlywood layer (compare the longitudinal moduli in Tab. 2).

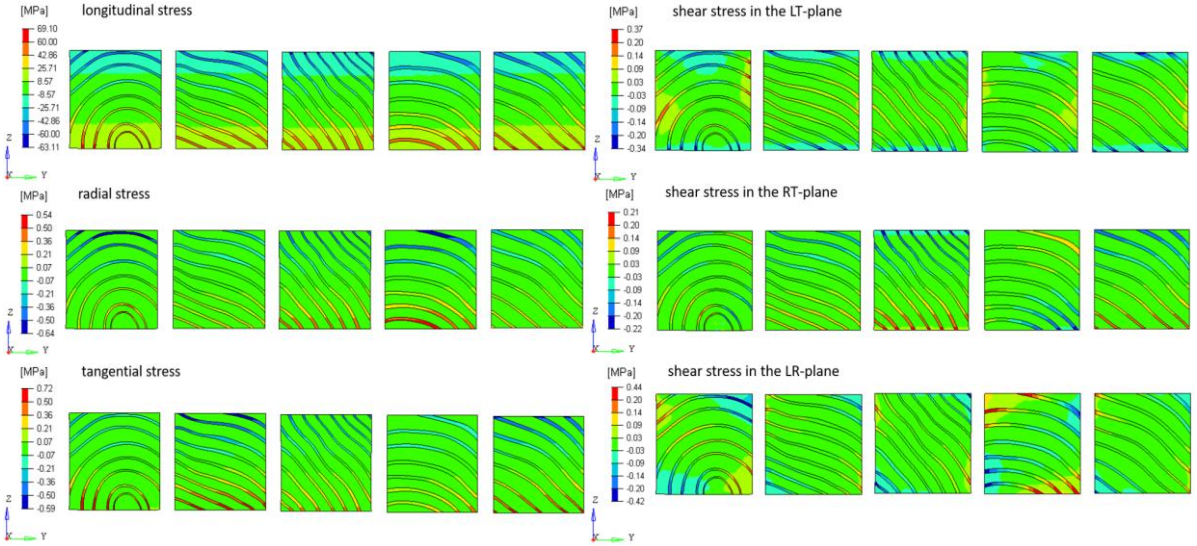

Fig. 7: Stresses in the 40 x 40 x 800 mm timber beams (under the loading F = 1250 N on the half model), middle section close-up view: a) normal stresses, b) shear stresses.

The presence of shear stresses is almost not noticeable at this loadcase and their distribution strongly depends on the annual ring pattern. The shear stress distribution in some of the specimens is shown in Fig. 7b. It can be observed in the specimens that shear stresses in earlywood are rather constant in the entire cross-section, while in latewood there are some stress hot-spots. Shear stresses in the TL- and LR-plane tend to show higher values the in the RT-plane. The results of further FE models are not shown. In order to have a complete overview of all the relevant data, Tab. 5 and Tab. 6 were created.

CONCLUSIONS

Depending on the task, the analysis of wooden structures can be done on different anatomical scales: from atomic through micro -microfibrils- or meso -growth rings-to macro- the wooden bulk itself. By the numerical modeling of wood used as a construction material, it is a more appropriate way to investigate its macroscopic properties.

The results gained through experiments give a better understanding of the behavior of timber beams under loading. The aim was to reconstruct the experiments by using the photos of end grains and creating unique FE models of timber beams, which lead to an outcome shown by the experiments. As for any other modeling approach, a major issue lies in the determination of the necessary mechanical properties. As the model performance and prediction capacity is highly dependent on these properties.

In this paper, two hypotheses have been introduced, with the help of which, the measurement results can be reproduced by finite element simulation. The first one states, that for high quality wood we can assume, that the surface and volume ratios of the earlywood and latewood nearly equals in all cross-sections along the longitudinal axis of the beam. The second one introduces empirical formulas for the orthotropic material properties with the help of the ROM-relation and the correlation among the material properties and density of earlywood and latewood.

The results of the compared measurements and FE calculations show a good correlation within the linear elastic limit. Obtaining data in the nonlinear range require further investigation. However, using the obtained information presented in this paper, further research about the fracture model is on the way, which is also adapted from the topic of fiber-reinforced materials and develops the presented material model even further. Its purpose is to describe the failure mode of wooden beams, and to predict the location of failure in advance.

REFERENCES

1. Andor, K., Lengyel, A., Polgár, R., Fodor, T., Karácsonyi, Z., 2015: Experimental and statistical analysis of spruce timber beams reinforced with CFRP fabric. Construction and Building Materials 99: 200-207
2. Sandhaas, C., van de Kuilen., J.W.G, 2013: Material model for wood. Heron 58(2-3): 171-191.
3. DIN EN 408-2012-10, 2012: Timber structures. Structural timber and glued laminated timber. Determination of some physical and mechanical properties.
4. Fleischmann, M., 2005: Numerische Berechnung von Holzkonstruktionen unter Verwendung eines realitätsnahen orthotropen elasto-plastisches Werkstoffmodells (Numerical calculation of timber structures using a realistic orthotropic elasto-plastic material model). PhD Dissertation. Technische Universität Wien, 184 pp, (in German).
5. Gecys, T., Daniunas, A., Bader, T.K., Wagner, L., Eberhardsteiner, J., 2015: 3D finite element analysis and experimental investigations of a new type of timber beam-to-beam connection. Engineering Structures 86: 134-145.
6. Gereke, T., Hering, S., Niemz, P., 2015: Finite element analysis of wood adhesive joints. Pro Ligno 12(1): 13-14.
7. Gibson, L.J. Ashby, M.F., 1997: Cellular solids: Structure and properties. Cambridge University Press, 510 pp.
8. Jernkvist, L.O., Thuvander, F., 2001: Experimental determination of stiffness variation across growth rings in *Picea abies*. Holzforschung 55(3): 309-317.
9. Nairn, J.A., 2006: Numerical simulations of transverse compression and densification in wood. Wood a Fiber Science 38(4): 576-591.
10. Khokhar, A., Zhang, H., Ridley-Ellis, D., Moore, J., 2010: The shear strength and failure modes of timber joists obtained from the torsion test method. Pp 20-24, 11th World Conference on Timber Engineering 2010.
11. Isaac, M.D., Ori, I., 2006: Engineering Mechanics of Composite Materials. (Second ed.) Oxford University Press, 464 pp.
12. Modén, C.S., Berglund, L.A., 2008: A two-phase annual ring model of transverse anisotropy in softwoods. Composites Science and Technology 68(14): 3020-3026.
13. Moshtaghin, A.F., Franke, S., Keller, T.P., Vassilopoulos, A., 2021: Experimental investigation of mesoscale variability of clear spruce mechanical properties in the radial direction. Construction and Building Materials 270: 121401.

14. Nilsen, T.S., 2015: Numerical modelling of wood microstructure. Master Thesis. Norwegian University of Science and Technology, NTNTU Trondheim, 7-12 pp.
15. Ormarsson, S., Dahlblom, O., Johansson, M., 2008: Finite element study of growth stress formation in wood and related distortion of sawn timber. Wood Science and Technology 43: 387-403.
16. Polgár, R., 2017: Offer for the quantitative determination of selection of stacked wood photo analytical processing algorithm by using spline functions. PhD Dissertation. West Hungarian University, 23-44 pp.
17. Qing, H., Mishnaevsky, Jr. L., 2010: 3D multiscale micromechanical model of wood: From annual rings to microfibrils. International Journal of Solids and Structures 47(9): 1253-1267.
18. Ross, R.J., 2010: Wood handbook: Wood as an engineering material. Centennial ed. General technical report FPL-GTR-190. Madison WI, U.S. Dept. of Agriculture. Forest Service, Forest Products Laboratory, 509 pp.
19. Saad, K., Lengyel, A., 2021: Inverse calculation of timber-CFRP composite beams using finite element analysis. Periodica Polytechnica Civil Engineering: 65(2): 437–449.
20. Salmén, L., Megistris, F.D., 2008: Finite element modelling of wood cell deformation travsverse to the fibre axis. Nordic Pulp and Paper Research Journal 23(2): 240-246.
21. Shao, B., Lewis, N., Fischer, A., Huang, Y., Lancelot, F., 2020: Parameters identification for wood material (*MAT143) and its application on the modeling of a typical timber nuki joint. 16th International LS-DYNA® Users Conference, 16 pp.
22. Abaqus, 2014: Analysis User's Manual, Version 6.14, Dassault Systèmes Simulia Corp.
23. Szalai, J., 1994: A faanyag és faalapú anyagok anizotróp rugalmasság- és szilárdságtana, 1. rész: A mechanikai tulajdonságok aniztrópiája (Anisotropic elasticity and strength of wood and wood-based materials, Part 1: Anisotropy of mechanical properties). Hillebrand Press. Sopron, Pp 38-127. (In Hungarian).
24. Warnet, L., Akkerman, R., 2008: Composite mechanics handouts. Pp 19-36, University of Twente.
25. Zhu, X., 2014: Nondestructive testing and system reliability based on finite element modeling in GFRP-reinforced timber beams. BioResources 9(3): 5501-5510.

TAMÁS KIRÁLY*, ZSOLT KARÁCSONYI, RUDOLF POLGÁR
UNIVERSITY OF SOPRON
INSTITUTE FOR APPLIED MECHANICS AND STRUCTURES
BAJCSY-ZSILINSZKY U. 4
H-9400 SOPRON
HUNGARY
*Corresponding author: tamas.kiraly1990@gmail.com